Geophysical Research Letters

RESEARCH LETTER
10.1029/2020GL090827

Analytical Prediction of Seismicity Rate Due to Tides and Other Oscillating Stresses

Elías R. Heimisson[1] **and Jean-Philippe Avouac**[1]

[1]Division of Geological and Planetary Sciences, California Institute of Technology, Pasadena, CA, USA

Key Points:
- We derive a simple analytical model for seismicity rate based on rate-and-state friction
- The model can be applied to perpetually oscillating stresses on Earth and other solid-surface bodies
- We reevaluate recent work on possible tidally triggered seismicity on Mars

Correspondence to:
E. R. Heimisson,
eheimiss@caltech.edu

Citation:
Heimisson, E. R., & Avouac, J.-P. (2020). Analytical prediction of seismicity rate due to tides and other oscillating stresses. *Geophysical Research Letters*, *47*, e2020GL090827. https://doi.org/10.1029/2020GL090827

Received 16 SEP 2020
Accepted 12 NOV 2020
Accepted article online 20 NOV 2020

Abstract Oscillatory stresses are ubiquitous on Earth and other solid-surface bodies. Tides and seasonal signals perpetually stress faults in the crust. Relating seismicity to these stresses offers fundamental insight into earthquake triggering. We present a simple model that describes seismicity rate due to perpetual oscillatory stresses. The model applies to large-amplitude, nonharmonic, and quasiperiodic stressing. However, it is not valid for periods similar to the characteristic time t_a. We show that seismicity rate from short-period stressing scales with the stress amplitude, but for long periods with the stressing rate. Further, that background seismicity rate r is equal to the average seismicity rate during short-period stressing. We suggest that $A\sigma_0$ may be underestimated if stresses are approximated by a single harmonic function. We revisit Manga et al. (2019, https://doi.org/10.1029/2019GL082892), which analyzed the tidal triggering of marsquakes and provide a rescaling of their seismicity rate response that offers a self-consistent comparison of different hydraulic conditions.

Plain Language Summary The surface of Earth and many other planets and moons is constantly being stressed in an oscillatory manner, for example, by the gravitational pull of moons, planets, and suns. Further, weather, climate, oceans, and other factors may also generate oscillatory stresses. The resulting fluctuations in stress may result in an increased or decreased probability of earthquakes with time. Here we derive a simple formula that can help scientists understand how these oscillatory stresses relate to seismic activity. Moreover, we revisit a recent estimate of the maximum sensitivity of marsquakes to tides and reach a different conclusion.

1. Introduction

Faults in the shallow crust are subject to perpetual, quasiperiodic, oscillatory stress perturbations due to several forcing factors. In particular, oceanic or solid earth tides, seasonal surface loads due to surface hydrology and the cryosphere, and surface temperature changes. The study of the seismicity response to such stress variations can in principle provide insight into fault friction and earthquake nucleation mechanisms (e.g., Ader et al., 2014; Beeler & Lockner, 2003; Luo & Liu, 2019; Scholz et al., 2019) and possibly inform us of the preparatory phase to impending earthquakes (e.g., Chanard et al., 2019; Tanaka, 2012). Stresses from oscillatory loading are often temporally complex but can be computed with reasonable accuracy (e.g., Agnew, 1997; Johnson et al., 2020; Lu et al., 2018; Tanaka et al., 2015; Tsuruoka et al., 1995), and their relationship to changes in seismicity or tremor rate might reveal fundamental insight into earthquake triggering. On Mars and the Moon, such factors might be the dominant source of seismicity (Duennebier & Sutton, 1974; Lognonne, 2005; Manga et al., 2019).

Although earthquakes are often weakly correlated to tides, tectonic tremors seem strongly correlated to tides both in the roots of strike-slip faults (Thomas et al., 2009, 2012) and subduction zones (Houston, 2015; Rubinstein et al., 2008; Yabe et al., 2015) where slow slip also is modulated by tidal stresses (Hawthorne & Rubin, 2010). Seasonal variation of seismicity driven by surface load variations has been reported in several studies (e.g., Amos et al., 2014; Bettinelli et al., 2008; Ueda & Kato, 2019). However, in most places, the seismicity rate depends weakly on tides (Cochran et al., 2004; Tanaka et al., 2002), except at mid-ocean ridges (e.g., Tolstoy et al., 2002). With the emergence of the next generation of machine-learning and template-matching techniques for generating earthquake catalogs, which may have 10 times the sensitivity of traditional methods (e.g., Ross et al., 2019), we will be able to detect and quantify the seismicity response to tidal and seasonal loading. New developments in observational earthquake seismology, and the emplacement of a seismometer on Mars, call for a simple model for seismicity rate under tidal loading that can be

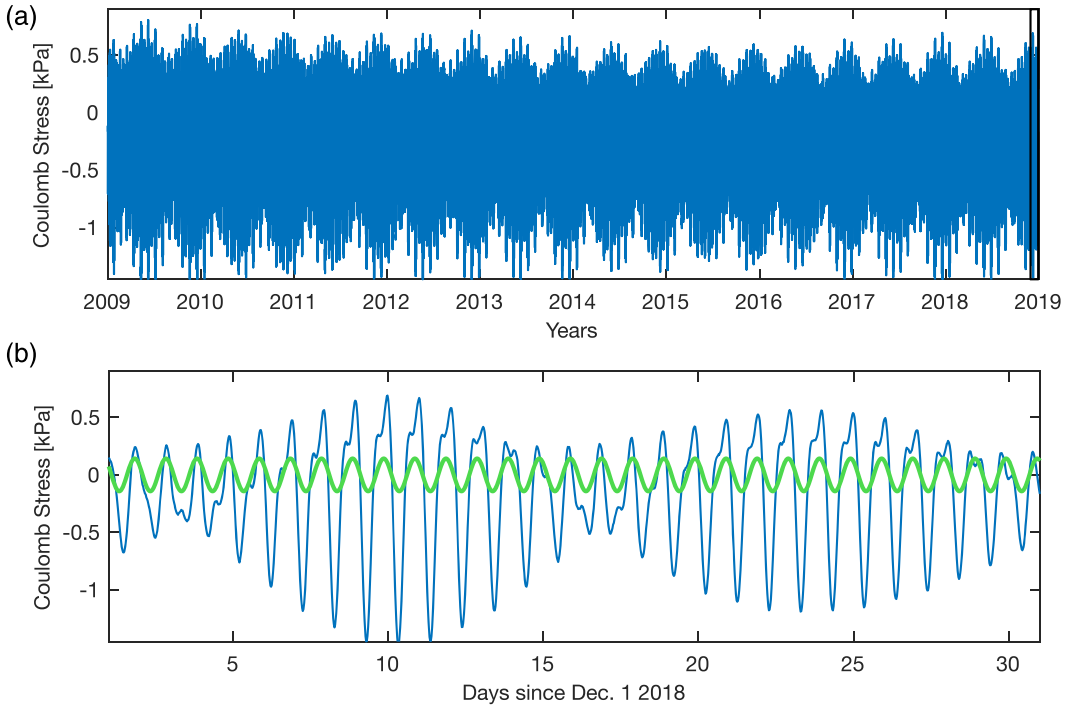

Figure 1. Time series of Coulomb stress changes due to the solid earth tides. (a) Ten years of Coulomb stress perturbations due to solid earth tides on a shallow right-lateral strike-slip fault striking NW-SE and located at Caltech campus. (b) The stress changes in the black box in (a) in blue, green represents the dominant single harmonic mode of the Coulomb stress time series. In section 3.1 we will compute the theoretical seismicity rate during the period in (b) where the entire time series in (a) is used to fade out the instantaneous initial response.

compared to data. Here we provide such a model (Equation 8) that can be readily used and has, in practice, only one free parameter in most applications. Further, we highlight important assumptions, such as ignoring finite fault effects and discuss potential pitfalls in applying rate-and-state seismicity production models to oscillatory stresses.

Theoretical studies have used the rate-and-state seismicity production model of Dieterich (1994) to develop an approximate theory for oscillatory stresses. Dieterich (2007) recognized that for small-amplitude and short-duration stress changes, the tidally induced signal could be approximated as the instantaneous response predicted by the Dieterich (1994) theory. Under these assumptions, Dieterich (2007) derived a simple relationship for a harmonic stress perturbation. Ader et al. (2014) provided a more general analytical expression; however, the analysis of Ader et al. (2014) was also restricted to a single harmonic perturbation. Because rate-and-state friction is nonlinear, knowing that the response to harmonic perturbations is not sufficient to describe the response to oscillatory stress variations in general. For example, tidal loading cannot be explained by a single harmonic perturbation (e.g., Figure 1), and the formalism of Dieterich (2007) and Ader et al. (2014) would not allow estimating the expected seismicity response. We, therefore, present a simple approximate relationship for seismicity rate due to arbitrary long-term oscillatory stressing that is superimposed on the long-term constant stressing rate. The oscillatory stressing can be nonharmonic and quasiperiodic and include random variations. The approximation is valid as long as the average of the oscillatory stress converges to a mean value on a time scale shorter than a characteristic time t_a. We give a mathematical condition for when the approximation is valid and provide corrections and alternative expressions for end-member cases where the approximation breaks down. As an illustration, we revisit the analysis of the seismicity response to tidal forcing on Mars of Manga et al. (2019), based on the solution of Dieterich (1994).

2. Theory

In this section, we present a simple model for triggering due to oscillatory stresses. We refer the reader to Appendix A1 for the details of the derivation.

Heimisson and Segall (2018) rederived the Dieterich (1994) theory and showed

$$R(t) = r\frac{K(t)}{1 + \frac{1}{t_a}\int_0^t K(t')dt'}, \tag{1}$$

where $R(t)$ is the seismicity rate produced by a population of seismic sources with background seismicity rate r. Further, $t_a = A\sigma_0/\dot{s}_0$ is a characteristic time over which fluctuations in seismicity rate return to the background seismicity, and A is a constitutive parameter proportional to the instantaneous frictional dependence on rate. If changes in normal stress $\sigma(t)$ are small compared to the initial normal stress σ_0, then K is well approximated as

$$K(t) \approx \exp\left(\frac{S(t)}{A\sigma_0}\right). \tag{2}$$

However, see Equation 30 in Heimisson and Segall (2018) for detailed conditions. $S(t) = \tau(t) - \mu\sigma(t)$ and $\dot{s}_0 = \dot{\tau}_r - \mu\dot{\sigma}_r$ are the modified Coulomb stressing history and background stressing rate, respectively, with $\mu = \tau_0/\sigma_0 - \alpha$ where α is the Linker and Dieterich (1992) constant, typically between 0 and 0.25 and describes coupling of normal stress and state. It is worth emphasizing that μ thus does not represent a coefficient of friction in the traditional sense, hence the name modified Coulomb stress.

The population of seismic sources is assumed to be noninteracting; however, Heimisson (2019) showed that an interacting population could be modeled as an equivalent noninteracting population. This means that we don't expect interaction on average to fundamentally change the response of the system to perturbations.

The presence of the integral in Equation 1 and the fact that $K(t) > 0$ causes perturbations introduced at $t = 0$ to decay. The short time limit of Equation 1, when the integral is much smaller than t_a, is the instantaneous response due to a perturbation in stress:

$$R = rK(t) \approx r\exp\left(\frac{S(t)}{A\sigma_0}\right). \tag{3}$$

Dieterich (2007) argued that the instantaneous response (Equation 3) is appropriate for periodic loading when the period T is small compared to a characteristic time, which describes when the seismicity rate starts decaying; in other words, the onset of the "Omori" ($\sim 1/t$) decay following a step change in stress. In Appendix A1, we investigate the validity of that argument by Dieterich (2007), which has often been applied the tidal triggering of seismicity and tremor (e.g., Delorey et al., 2017; Dieterich, 2007; Scholz et al., 2019; Thomas et al., 2012). In Appendix A1, we show for a time-dependent stressing history of the form $S(t) = S_T(t) + \dot{s}_0 t$, where $S_T(t)$ is an oscillatory modified Coulomb stress with a well-defined average value (e.g., tidally induced stress), the long-term response in seismicity rate is

$$\frac{R(t)}{r} = \frac{\exp\left(\frac{S_T(t)}{A\sigma_0}\right)}{M}, \tag{4}$$

where M is the average

$$M = \lim_{T\to\infty}\frac{1}{T}\int_0^T \exp\left(\frac{S_T(t)}{A\sigma_0}\right)dt. \tag{5}$$

We note that $M = 1$ only if $S_T(t) = 0$. The average of $S_T(t)$ may be 0, but with nonzero amplitude, we always have $M > 1$. Equation 4 generalizes the special cases for a harmonic perturbation that was explored by Ader et al. (2014). One important consequence of Equations 4 and 5 is that the average seismicity rate $\bar{R}(t)$ under oscillatory stresses is the same as the background rate r when no oscillatory stresses occur. This can be shown explicitly:

$$\frac{\bar{R}(t)}{r} = \lim_{T\to\infty}\frac{1}{T}\int_0^T \frac{R(t)}{r}dt = \frac{1}{M}\lim_{T\to\infty}\frac{1}{T}\int_0^T \exp\left(\frac{S_T(t)}{A\sigma_0}\right)dt = 1. \tag{6}$$

In other words, in the presence of general oscillatory stresses, the background rate, in the traditional sense expressed by Dieterich (1994), is observable as the average seismicity rate. This finding is consistent with

Equation 55 derived by Helmstetter and Shaw (2009), which shows that earthquake number is linearly proportional to the stress change at $t \gg t_a$ and thus a zero mean stress change would not induce any change in a number of events, for an observation time much longer than t_a. However, Equation 6 is more general since it doesn't assume that the mean stress is 0.

Let's define t_0 as a zero-crossing time of the oscillatory stress perturbation, that is, $S_T(t_0) = 0$. Then the rate is

$$R_0 = \frac{r}{M}. \tag{7}$$

It can thus be useful to rewrite Equation 4

$$R(t) = R_0 \exp\left(\frac{S_T(t)}{A\sigma_0}\right). \tag{8}$$

Rate R is equal to the background average rate r when there are no oscillatory stresses (i.e., $R_0 = r$ if $M = 1$); thus, the approximation proposed by Dieterich (2007) (Equation 3) is valid when the stress perturbation is very small compared to $A\sigma_0$ ($|S_T(t)|/A\sigma_0 \ll 1$); otherwise, it remains valid within a scaling factor M. If $M > 1$ the peak-to-peak variation of the seismicity can be significantly overestimated. For many applications, the assumption $|S_T(t)|/A\sigma_0 \ll 1$ is valid. In applications to aftershocks $A\sigma_0 \sim 0.01$–0.1 MPa (Hainzl, Steacy, et al., 2010), which is much larger than tidal stresses ($\sim 10^{-3}$ to 10^{-4} MPa, e.g., Figure 1). However, tidal triggering of tectonic tremors near Parkfield has suggested an average value of $A\sigma_0 = 6 \cdot 10^{-4}$ MPa (Thomas et al., 2012), in which case $S_T(t)/A\sigma_0$ could be on the order of 0.2–2. So the $S_T(t)/A\sigma_0 \ll 1$ assumption is clearly violated. Furthermore, $A\sigma_0$ may be generally different on other planetary bodies compared to Earth (Manga et al., 2019).

It is useful to summarize the fundamental underlying assumptions that give rise to Equation 4 or 8:

1. The average in Equation 5 should converge on a time scale much less t_a.
2. Oscillatory stresses $S_T(t)$ have been ongoing for a time much larger than t_a.
3. Normal stress changes should be modest compared to initial normal stress for the Coulomb stress approximation to be valid (Heimisson & Segall, 2018).
4. Other assumptions of the Dieterich (1994) theory, most importantly, source finiteness can be neglected (see Kaneko & Lapusta, 2008), the population of seismic sources is well above steady state (see Heimisson & Segall, 2018) and neglecting effects that arise from source interactions (see Heimisson, 2019).

Additional discussion of these assumptions is provided in Appendices A1 and B1, but it is worth highlighting here a fundamental difference that arises when the period of oscillations is much larger than t_a, and Assumption 1 is strongly violated, in which case the seismicity rate is proportional to the stressing rate, not the stress:

$$\frac{R(t)}{r} \approx \frac{1}{1 - t_a \frac{\dot{S}_T(t)}{A\sigma_0}}. \tag{9}$$

One can interpret Equation 9 such that long-period stresses effectively change the background rate to $r'(t) = r/(1 - t_a \dot{S}_T(t)/(A\sigma_0))$ because the populations of seismic sources can evolve to a new steady-state rate on time scales larger than t_a. In Appendix B1 we show how a combination of (4) and (9) can be used when long-period and short-period stressing is superimposed (see Equation B6).

3. Examples of Applications and Comparison With Theory

3.1. Application to Solid Earth Tides

To test Equation 4 against the full solution (Equation 1), we generate a time series of Coulomb stress change using the *Solid* software (Milbert, 2018) representing the (modified) Coulomb stress changes, with $\mu = 0.4$, due to the solid earth tides on shallow right-lateral strike-slip fault striking NW-SE and located at Caltech campus in California. The entire time series is shown in Figure 1a, but we will restrict our attention to the observation window shown in Figure 1b. Most of the time series in Figure 1a is used to erase the initial response or initial conditions in Equation 1 and compute M. In the following we refer to this procedure simply as erasing the initial response. We choose $t_a = 0.5$ years. We vary $A\sigma_0$ as described in

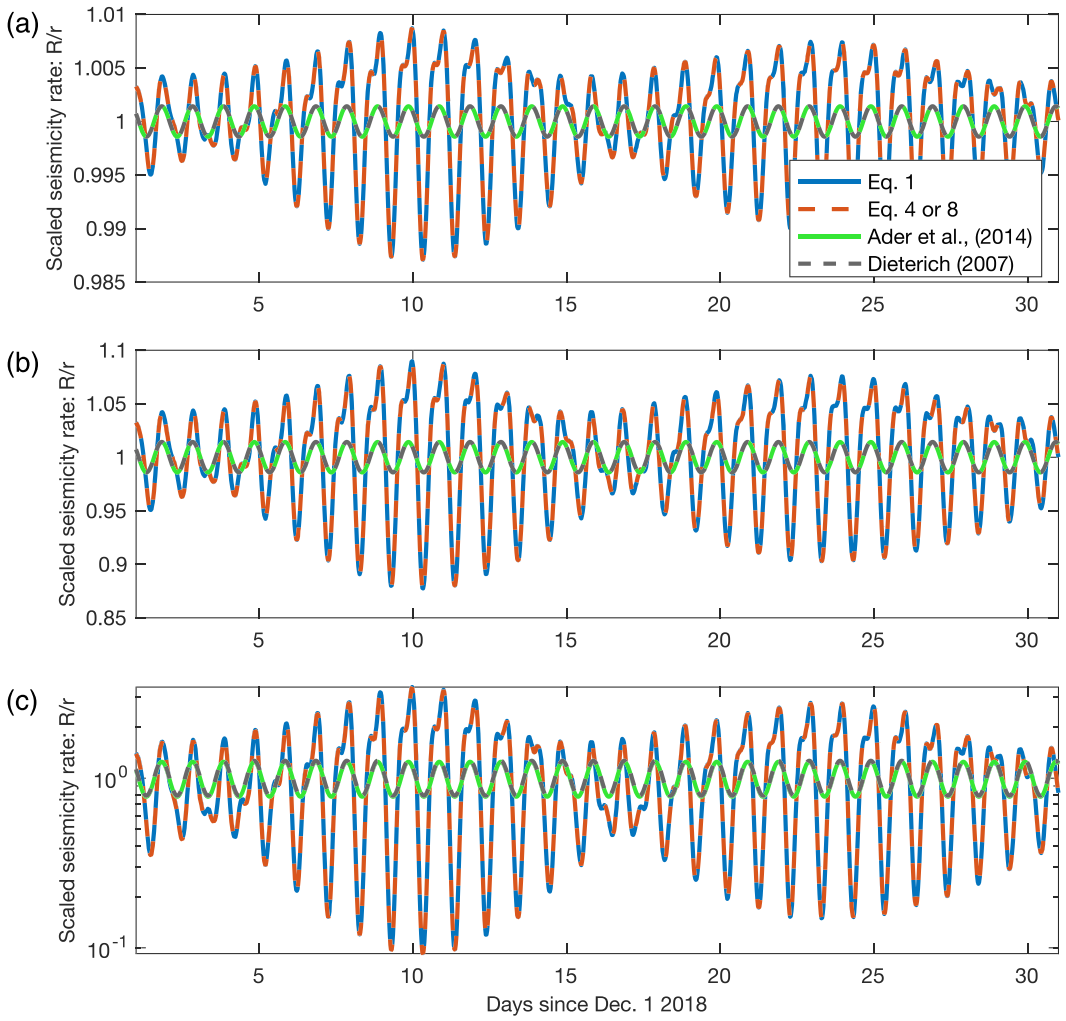

Figure 2. Comparison of various approximations and the full solution in Equation 1 after the initial response has been faded out. Scaled seismicity rate (R/r) for (a) $A\sigma_0 = 1 \cdot 10^{-1}$ MPa, (b) $A\sigma_0 = 1 \cdot 10^{-2}$ MPa, (c) $A\sigma_0 = 6 \cdot 10^{-4}$ MPa (note the logarithmic scale). In all cases, Equation 4 provides an excellent approximation with an average relative error of less than (a) 0.002%, (b) 0.02%, and (c) 0.7%. A single harmonic perturbation does not capture the details of the curve shape or amplitude.

Figure 2 choosing values that reflect a typical range of values in aftershock studies: 0.1 and 0.01 MPa (Hainzl, Steacy, et al., 2010) and a value inferred in studying tidal triggering of tectonic tremors $6 \cdot 10^{-4}$ MPa (Thomas et al., 2012). We find that even for large fluctuations in R/r, Equation 4 is in good agreement with the full solution (Figure 2c).

Corresponding theory for a single harmonic stress perturbation of Dieterich (2007) is obtained from Equation 3 by representing $S_T(t)$ by a single harmonic function. Likewise, the harmonic theory of Ader et al. (2014) is obtained in the same manner from Equation 4. We computed the dominant frequency of the signal in Figure 1a by computing a power spectral density. Then find the best fitting amplitude and phase by minimizing an L_2 norm that quantifies the residual between the time series shown in Figure 1a and the single harmonic function. The resulting harmonic stress perturbation is shown in Figure 1b in green and is used to compute the seismicity rate using both the expressions from Dieterich (2007) and Ader et al. (2014) in Figure 2. The dominant frequency of the earth tide signal generally predicts when the seismicity rate is higher or lower than average. However, the shape and amplitude of the theoretical seismicity rate time series cannot be matched with a single harmonic function.

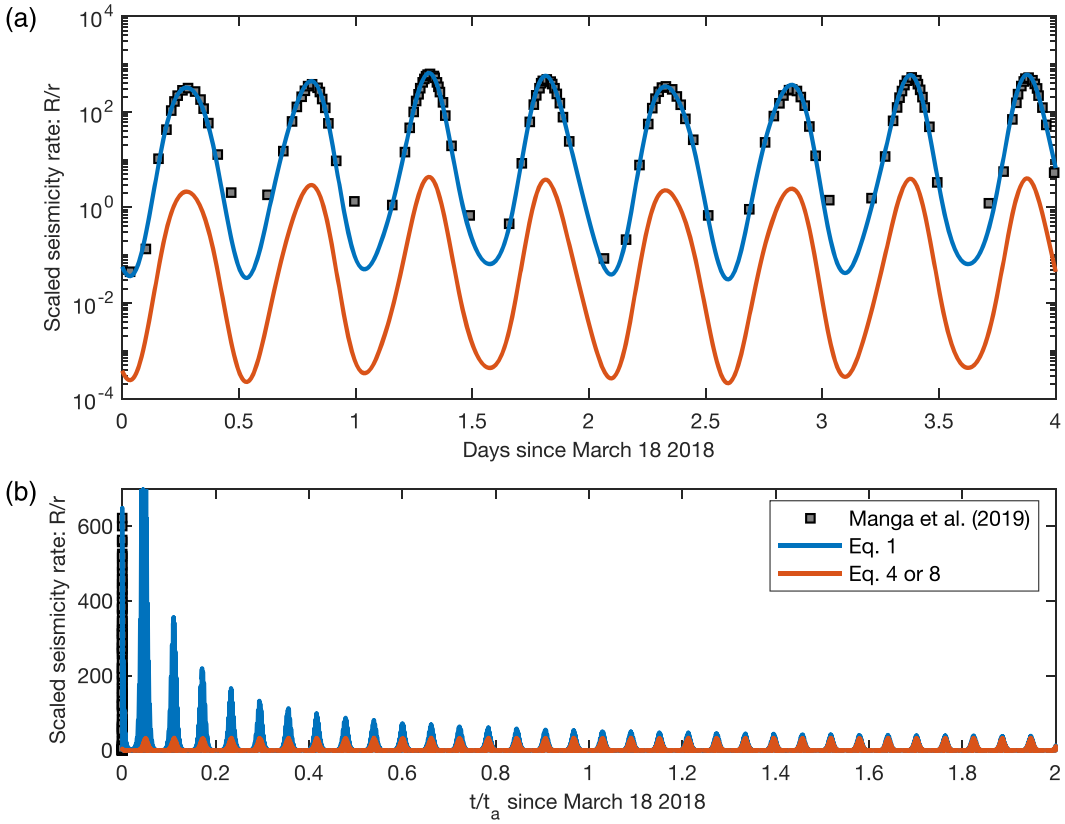

Figure 3. Reevaluation of Manga et al. (2019) reveals that they likely overestimated the maximum response by at least a factor of 10. (a) Using an approximate stressing history, we observe that Equation 1 is in good agreement with the results reported in Figure 3 bottom-left panel in Manga et al. (2019). In contrast, Equation 4 suggests that the amplitude should be approximately 100 times less although the shape of the curves is the same. (b) Simulating a time scale $t \sim t_a$ where $t_a \approx 71.5$ Earth years, which we computed based on parameters given by Manga et al. (2019), shows that Equations 1 and 4 converge once the initial response gets erased.

3.2. Marsquakes: Reevaluating Manga et al. (2019)

Recently, Manga et al. (2019) argued that Mars might have a clearer relationship between tides and seismicity rate, which could result in variation as large as 2 orders of magnitude in scaled seismicity rate R/r, also referred to as relative seismicity rate (see Figure 3, bottom-left panel in Manga et al., 2019). Their predicted signal was apparently produced based on the initial instantaneous response (Figure 3a) and thus not strictly correct, as presented. As discussed in the previous section, care needs to be taken to erase the initial response when applying Equation 1 by simulating a time window before the observation window that is much larger than t_a and is sufficiently long to estimate M accurately. If this is not done, the tidal response may be significantly overestimated, indeed by a factor of $1/M$.

We use Equation 1 without erasing the initial response and find a good agreement with their results (Figure 3a), despite some simplifying assumptions that are detailed in the next paragraph. Extrapolation of their results suggests that the changes in seismicity rate should be much smaller than they estimated (Figure 3b).

To replicate the results of Manga et al. (2019), we approximate the Coulomb stress perturbations they reported for strike = 0° (Figure 2 in Manga et al., 2019) by a sum of three harmonic functions fitted to a digitized version of their figure. This provides an excellent fit to the reported Coulomb stress calculations during the 4 day window they show. However, the long-term extrapolation in Figure 3b shows that the seismicity rate decays over a time scale of $t \sim t_a$, before reaching the expected rate variation due to tidal loading that would be observable.

Fortunately, the ratio between the instantaneous response and the long-term response is M. Thus, from Equation 8 we can conclude that the reported relative rate of Manga et al. (2019) is correct if interpreted as relative to R_0, but not r as they stated. One important consequence is that the difference in seismicity rate shown in different panels in Figure 3 in Manga et al. (2019) (showing response due to variations in effective normal stress) does not reflect relative changes in absolute seismicity rate. In their top panels $M \approx 1$, in the bottom panels $M \approx 100$. The maximum rate in the bottom panel is ≈600, but for the top ≈1. Thus, the difference in maximum absolute seismicity rate, of the two scenarios, is only about a factor of 6.

4. Discussion

Equation 4 or 8 offers an estimate of the seismicity rate produced by a population of seismic sources due to a stressing history produced by a constant stressing rate and oscillating stress sources. These equations are perfectly equivalent and simple to use; given that the stressing history is known, there is only one free parameter that may need to be fitted: $A\sigma_0$. The results thus offer a way to assess the validity of rate-and-state seismicity rate theories (Dieterich, 1994; Heimisson & Segall, 2018) and place constraints on the friction law. Further, estimating $A\sigma_0$ by using tides or seasonal stress variations has implications for physics-based forecasts of aftershocks, where this parameter also needs to be estimated (e.g., Hainzl, Brietzke, et al., 2010). Thus, tides could be used in advance to or map spatial variations of this parameter. Those values could then be used for aftershock forecasts once an earthquake occurs or forecast-induced seismicity expected in response to anthropogenic stress changes.

Equation 8 may be preferred in some data applications compared to Equation 4. Remarkably, Yabe et al. (2015) and Scholz et al. (2019) successfully applied Equation 8 in good agreement with data without explicit theoretical underpinnings. While Yabe et al. (2015) correctly state that R_0 is a reference rate when tidal stress is 0, the latter study refers to R as "the instantaneous seismicity rate." We have shown here that R in Equation 3 represents the instantaneous seismicity rate, but Equation 8 is the approximate seismicity rate in the presence of long-term response tidal loading or other oscillatory stresses. $R_0 \neq r$, unless $|S_T(t)|/A\sigma_0 \ll 1$ for all t, in which case $R_0 \approx r$.

The approximation made in Equation 4 or 8 is not valid in the limit of a very long period stress variations that are larger than t_a, as described by Equation 9. In this case, we expect the seismicity rate to be proportional to the stressing rate, but not the stress. Beeler and Lockner (2003) conducted experiments on a saw-cut sample in a triaxial loading frame. They imposed oscillatory stresses on a constant stressing rate and found that for short periods compared to the nucleation time, changes in event probability was in phase with the stress. However, for long periods the probability of events was proportional to and in phase with the stressing rate. Their finding is in agreement with our theoretical results.

Johnson et al. (2017) investigated the relationship between seismicity rate and seasonal variations in shear stress and stress rate in California. Depending on fault orientation, they identified a weak correlation of seismicity rate with either shear stressing rate or stress. This finding would suggest that, on average, t_a changes with fault orientation. That is reasonable since background stressing rates must vary with fault orientation. We emphasize that when investigating seasonal changes in seismicity rate, which may be on a similar time scale as t_a, one must be careful since no approximation presented here may work. We strongly suggest that Equation 1 should be used for reference after erasing the initial response. Further, we recall that our analysis assumes that a single degree of freedom spring-and-slider system can approximate the response of a fault to a stress perturbation. Significant differences have been observed if finite fault effects need to be taken into account (e.g., Ampuero & Rubin, 2008; Kaneko & Lapusta, 2008; Rubin & Ampuero, 2005). Simulations indicate that this happens if the typical period of the stress perturbation is of the order of $2\pi t_a$ (Ader et al., 2014). In that case, the approximate analytical solutions described in this study would not apply.

Using a single harmonic function to represent the oscillating stressing history may be desirable due to the simplicity of the problem and the fact that spectral analysis, such as the Schuster spectra, can be used to extract the dominant period of the seismicity rate (Ader et al., 2014). However, this may lead to a bias in the estimate of $A\sigma_0$ if the stressing history has multiple components that can add up coherently. Let us assume that the stressing history is composed of N harmonic components:

$$S_T(t) = \sum_{i=1}^{N} c_i \sin\left(\frac{2\pi t}{T_i} + \phi_i,\right) \tag{10}$$

where the amplitudes are sorted: $c_1 > c_2 > \ldots > c_N$ and thus T_1 is the dominant period. Using Equation 8 and only the dominant harmonic component of the $S_T(t)$ then one finds

$$\log\left(\frac{\max(R)}{R_0}\right) = \frac{c_1}{(A\sigma_0)_{SH}}, \tag{11}$$

where $(A\sigma_0)_{SH}$ represents the estimate of $A\sigma_0$ under the assumption of a single harmonic, and $\max(R)$ is the maximum observed seismicity rate. However, for multiple harmonics we find

$$\log\left(\frac{\max(R)}{R_0}\right) = \max\left(\frac{\sum_{i=1}^{N} c_i \sin\left(\frac{2\pi t}{T_i} + \phi_i,\right)}{(A\sigma_0)_{MH}}\right) \leq \frac{\sum_{i=1}^{N} |c_i|}{(A\sigma_0)_{MH}}, \tag{12}$$

where $(A\sigma_0)_{MH}$ represents the estimate of $A\sigma_0$ under the assumption of multiple harmonics. Thus, we conclude that the ratio of the two estimates is bounded in the following manner:

$$\frac{(A\sigma_0)_{MH}}{(A\sigma_0)_{SH}} \leq \frac{\sum_{i=1}^{N} |c_i|}{|c_1|}. \tag{13}$$

Therefore, we expect that $A\sigma_0$ is typically underestimated if a single harmonic stress source is assumed. This conclusion is consistent with Figure 2, which shows that the amplitude is not well match by a single harmonic. However, dividing $A\sigma_0$ by factor 5.3 would allow the single harmonic approximation to match the maximum rate of the full solution. Equation 13 thus successfully offers an inequality constraint of $(A\sigma_0)_{MH} \leq 30 \cdot (A\sigma_0)_{SH}$.

5. Conclusions

We have derived a simple approximate equation to quantify the relationship between seismicity and oscillatory stresses, based on assuming an earthquake nucleation process governed by rate-and-state friction. This relationship may be used, for example, in theoretical or observational studies of seismicity response to tidal and seasonal loading. For stress perturbations with periods shorter than t_a, Equation 4 or 8 provides an excellent approximation. We have also provided an approximation for periods longer than t_a (Equation 9). Finally, in Appendix B1 and Equation B6 we offer an approximation for superposition of short-period loading and long-period loading relative to t_a. However, for stress perturbations with periods $\sim t_a$ require a more careful analysis (e.g., Equation 1).

Appendix A: Derivation of Equation 4

We write the stressing history as the sum of steady stressing rate $(\dot{s}_0 t)$ and time-dependent stress perturbation $S_T(t)$, that is, $S(t) = S_T(t) + \dot{s}_0 t$ and obtain

$$K(t) = \exp\left(\frac{S(t)}{A\sigma_0}\right) = \exp\left(\frac{S_T(t)}{A\sigma_0} + \frac{t}{t_a}\right) = \eta(t)\exp\left(\frac{t}{t_a}\right). \tag{A1}$$

We assume $\eta(t)$ is a function with the following property:

$$\eta(t) = M + \epsilon(t), \text{ where } M = \lim_{T\to\infty}\frac{1}{T}\int_0^T \eta(t)dt \text{ with } |M| < \infty, \tag{A2}$$

it follows that

$$\lim_{T\to\infty}\frac{1}{T}\int_0^T \eta(t)dt = \lim_{T\to\infty}\frac{1}{T}\int_0^T Mdt + \frac{1}{T}\int_0^T \epsilon(t)dt = M + \lim_{T\to\infty}\frac{1}{T}\int_0^T \epsilon(t)dt. \tag{A3}$$

In other words, M is the average of $\eta(t)$ and $|M| < \infty$; thus, the average of $\epsilon(t)$ is 0, that is,

$$\lim_{T\to\infty}\frac{1}{T}\int_0^T \epsilon(t)dt = 0. \tag{A4}$$

For example, any periodic bounded function $\eta(t) = \eta(t+T)$ satisfies these conditions. In this case, the physical interpretation of $\eta(t)$ is $\log(\eta(t)) = S_p(t)/A\sigma_0$ where $S_p(t) = S_p(t+T)$ is a periodic stress perturbation.

There is no requirement that $S_T(t)$ has to be a harmonic perturbation, such as previously explored (Ader et al., 2014; Dieterich, 2007), or a periodic perturbation. Tidal loading has multiple harmonic components and their periods do not exactly differ by an integer. The resulting stressing history is not periodic. However, we can still write $\eta(t) = \exp(S_T(t)/A\sigma_0) = M + \epsilon(t)$. Further, we could imagine that $\epsilon(t)$ contains a stochastic component with a well-defined zero mean. We shall now derive the long-term behavior of a population of seismic sources that is persistently subject to a stressing history that can be written in the form of Equation A1.

Once the integral in the denominator of Equation 1 is much larger than t_a, we may simplify

$$\frac{R(t)}{r} = \frac{K(t)}{\frac{1}{t_a}\int_0^t K(t')dt'}, \tag{A5}$$

or using the notation in Equation A1

$$\frac{R(t)}{r} = \frac{\eta(t)\exp\left(\frac{t}{t_a}\right)}{\frac{1}{t_a}\int_0^t \eta(t)\exp\left(\frac{t}{t_a}\right)dt'}. \tag{A6}$$

Substitution with A2 yields

$$\int_0^t \eta(t)\exp\left(\frac{t}{t_a}\right)dt' = t_a M\exp\left(\frac{t}{t_a}\right) + \int_0^t \epsilon(t')\exp\left(\frac{t'}{t_a}\right)dt' \tag{A7}$$

and we obtain:

$$\frac{R(t)}{r} = \frac{\eta(t)}{M + \frac{1}{t_a}\int_0^t \epsilon(t')\exp\left(\frac{-(t-t')}{t_a}\right)dt'}. \tag{A8}$$

We recognize that $\int_0^t \epsilon(t')\exp\left(\frac{-(t-t')}{t_a}\right)dt'$ is simply a convolution. The function $\exp(-(t-t')/t_a)$ imposes a memory effect and essentially eliminates any contribution in fluctuations in $\epsilon(t)$ in a time window of that lies significantly outside times $t - t_a$ to t. Thus, if $\epsilon(t)$ averages to 0 on a time scale that is significantly shorter than t_a, the integral can generally be ignored. For example, this condition is satisfied if the oscillatory stresses and possible random stresses, average to approximately 0 on a time scale smaller than t_a. More precisely, the integral can be ignored if the following condition applies:

$$\left|\frac{\frac{1}{t_a}\int_0^t \epsilon(t')\exp\left(\frac{-(t-t')}{t_a}\right)dt'}{M}\right| \ll 1, \text{ for all } t, \tag{A9}$$

then Equation A8 reduces to

$$\frac{R(t)}{r} = \frac{\eta(t)}{M} = \frac{\exp\left(\frac{S_T(t)}{A\sigma_0}\right)}{M}. \tag{A10}$$

Appendix B: Validity of Equation 4 or 8

Here we offer further analysis on the validity of Equation 4 or 8 and provide some insight into the regimes when they are not valid. The validity of Equation 4 or 8 rests on the validity of Equation A9. We investigate two different expansions of the relevant term through repeated integration by parts:

$$\frac{1}{t_a}\exp\left(-\frac{t}{t_a}\right)\int \epsilon(t')\exp\left(\frac{t'}{t_a}\right)dt' = \frac{\epsilon^{-1}(t)}{t_a} - \frac{\epsilon^{-2}(t)}{t_a^2} + \frac{\epsilon^{-3}(t)}{t_a^3} + \ldots \tag{B1}$$

$$\frac{1}{t_a}\exp\left(-\frac{t}{t_a}\right)\int \epsilon(t')\exp\left(\frac{t'}{t_a}\right)dt' = \epsilon - t_a\epsilon^1(t) + t_a^2\epsilon^2(t) - t_a^3\epsilon^3(t) + \ldots \tag{B2}$$

where ϵ^n is the nth derivative of ϵ and ϵ^{-n} is the nth indefinite integral (or antiderivative) of ϵ. If the largest period, T_{max} in the Fourier decomposition of ϵ with a nonzero coefficient satisfies $T_{max} < t_a$, then the nth

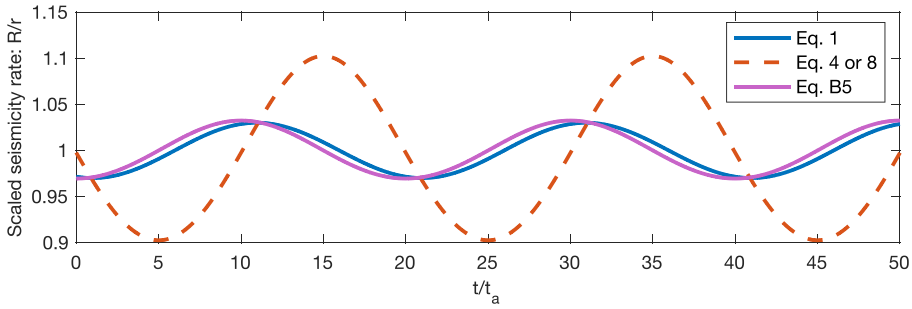

Figure B1. Simulations of seismicity rate response for $S_T(t)/A\sigma_0 = -0.1 \cdot \sin(2\pi t/T) + t/t_a$, where the period $T = 20t_a$. In this limit Equation 9 predicts that the seismicity rate should be in phase with the stressing rate and that Equation 4 or 8 is in no agreement with the full solution (1).

term in Equation B1 will be a correction of order $O(T^n_{max}/t^n_a)$, and convergence is expected. For long-period changes $T_{min} > t_a$, Equation B2 provides an expansion where we have $O(t^n_a/T^n_{min})$ correction for the nth term.

In the short-period limit, $T_{max} < t_a$, we find a first-order correction to Equation 4:

$$\frac{R(t)}{r} = \frac{\exp\left(\frac{S_T(t)}{A\sigma_0}\right)}{M + \frac{\epsilon^{-1}(t)}{t_a}}, \tag{B3}$$

where in practice we compute $\epsilon^{-1}(t)$ using the following equation, unless the indefinite integral is known analytically.

$$\epsilon^{-1}(t) = \int_{-t_0}^{t} \exp\left(\frac{S_T(t)}{A\sigma_0}\right) dt - Mt, \tag{B4}$$

where $t_0 > 0$ is chosen sufficiently large to erase the influence of the initial stress value in the integral. Numerical exploration of Equation B3 suggested that the additional correction term is typically small and unlikely to be useful in practical applications.

In the long-period limit, $T_{min} > t_a$, we get

$$\frac{R(t)}{r} = \frac{\exp\left(\frac{S_T(t)}{A\sigma_0}\right)}{\exp\left(\frac{S_T(t)}{A\sigma_0}\right) - t_a \exp\left(\frac{S_T(t)}{A\sigma_0}\right)\frac{\dot{S}_T(t)}{A\sigma_0}} = \frac{1}{1 - t_a\frac{\dot{S}_T(t)}{A\sigma_0}} \approx 1 + t_a\frac{\dot{S}_T(t)}{A\sigma_0}, \tag{B5}$$

where the approximation represents a first-order Taylor expansion. Equation B5 may be useful when investigating long-term behavior such as seasonal changes if t_a is shorter than 1 year as is probably the case in active tectonic settings (e.g., Bettinelli et al., 2008). Notably, Equation 9 depends on the stressing rate, not directly the stress, and is to the first order linearly proportional to the stressing rate (Figure B1), implying that, in this particular limit, the seismicity rate is out of phase with the stress variations. This result is consistent with the findings of Helmstetter and Shaw (2009) for slowly varying stresses. Furthermore, we see that Equation 4 is not valid in this limit since it predicts that the seismicity rate is proportional to the stress change, not the stressing rate.

Finally, we can infer seismicity rate behavior in the presence of both oscillatory stresses with short periods $S^S_T(t)$ and long periods $S^L_T(t)$ relative to t_a. Inspection of Equation B5 suggests that long-period stresses changes act to modulate the background rate. This suggests a combined form of Equations A10 and B5:

$$\frac{R(t)}{r} = \frac{\exp\left(S^S_T(t)\right)}{\frac{1}{M}\left(1 - t_a\frac{\dot{S}^L_T(t)}{A\sigma_0}\right)}, \tag{B6}$$

where M is the long-term mean of $\exp\left(S^S_T(t)\right)$, that is, the short-period stresses. While Equation B6 is derived here by inspection, it can be derived explicitly in the same manner as Equation B5 by assuming that the

long-period stresses long periods $S_T^L(t) + t/t_a$ can be considered constant at the time scale that $\exp(S_T^S(t))$ converges to a mean. This is essentially the same assumption as is required for Equation A10 to be valid.

Data Availability Statement

This is a theoretical paper and contains no data.

Acknowledgments
This research was partly supported by NSF award EAR-1821853. We thank three anonymous reviewers for their constructive remarks that significantly improved this manuscript.

References

Ader, T. J., Lapusta, N., Avouac, J.-P., & Ampuero, J.-P. (2014). Response of rate-and-state seismogenic faults to harmonic shear-stress perturbations. *Geophysical Journal International*, *198*(1), 385–413. https://doi.org/10.1093/gji/ggu144

Agnew, D. C. (1997). NLOADF: A program for computing ocean-tide loading. *Journal of Geophysical Research*, *102*(B3), 5109–5110. https://doi.org/10.1029/96JB03458

Amos, C. B., Audet, P., Hammond, W. C., Bürgmann, R., Johanson, I. A., & Blewitt, G. (2014). Uplift and seismicity driven by groundwater depletion in central California. *Nature*, *509*(7501), 483–486. https://doi.org/10.1038/nature13275

Ampuero, J.-P., & Rubin, A. M. (2008). Earthquake nucleation on rate and state faults—Aging and slip laws. *Journal of Geophysical Research*, *113*, B01302. https://doi.org/10.1029/2007JB005082

Beeler, N. M., & Lockner, D. A. (2003). Why earthquakes correlate weakly with the solid earth tides: Effects of periodic stress on the rate and probability of earthquake occurrence. *Journal of Geophysical Research*, *108*(B8), 2391. https://doi.org/10.1029/2001JB001518

Bettinelli, P., Avouac, J.-P., Flouzat, M., Bollinger, L., Ramillien, G., Rajaure, S., & Sapkota, S. (2008). Seasonal variations of seismicity and geodetic strain in the Himalaya induced by surface hydrology. *Earth and Planetary Science Letters*, *266*(3), 332–344. https://doi.org/10.1016/j.epsl.2007.11.021

Chanard, K., Nicolas, A., Hatano, T., Petrelis, F., Latour, S., Vinciguerra, S., & Schubnel, A. (2019). Sensitivity of acoustic emission triggering to small pore pressure cycling perturbations during brittle creep. *Geophysical Research Letters*, *46*, 7414–7423. https://doi.org/10.1029/2019GL082093

Cochran, E. S., Vidale, J. E., & Tanaka, S. (2004). Earth tides can trigger shallow thrust fault earthquakes. *Science*, *306*(5699), 1164–1166. https://doi.org/10.1126/science.1103961

Delorey, A. A., van der Elst, N. J., & Johnson, P. A. (2017). Tidal triggering of earthquakes suggests poroelastic behavior on the San Andreas fault. *Earth and Planetary Science Letters*, *460*, 164–170. https://doi.org/10.1016/j.epsl.2016.12.014

Dieterich, J. (1994). A constitutive law for rate of earthquake production and its application to earthquake clustering. *Journal of Geophysical Research*, *99*(B2), 2601–2618. https://doi.org/10.1029/93JB02581

Dieterich, J. H. (2007). 4.04—Applications of rate- and state-dependent friction to models of fault-slip and earthquake occurrence, (Second). In G. Schubert (Ed.), *Treatise on geophysics (second edition)*. Oxford: Elsevier, (pp. 93–110). https://doi.org/10.1016/B978-0-444-53802-4.00075-0

Duennebier, F., & Sutton, G. H. (1974). Thermal moonquakes. *Journal of Geophysical Research (1896-1977)*, *79*(29), 4351–4363. https://doi.org/10.1029/JB079i029p04351

Hainzl, S., Brietzke, G. B., & Zoller, G. (2010). Quantitative earthquake forecasts resulting from static stress triggering. *Journal of Geophysical Research*, *115*, B11311. https://doi.org/10.1029/2010JB007473

Hainzl, S., Steacy, S., & Marsan, D. (2010). Seismicity models based on Coulomb stress calculations. *Community Online Resource for Statistical Seismicity Analysis*. https://doi.org/10.5078/corssa-32035809, Retrieved from http://www.corssa.org

Hawthorne, J. C., & Rubin, A. M. (2010). Tidal modulation of slow slip in Cascadia. *Journal of Geophysical Research*, *115*, B09406. https://doi.org/10.1029/2010JB007502

Heimisson, E. R. (2019). Constitutive law for earthquake production based on rate-and-state friction: Theory and application of interacting sources. *Journal of Geophysical Research: Solid Earth*, *124*, 1802–1821. https://doi.org/10.1029/2018JB016823

Heimisson, E. R., & Segall, P. (2018). Constitutive law for earthquake production based on rate-and-state friction: Dieterich 1994 revisited. *Journal of Geophysical Research: Solid Earth*, *123*, 4141–4156. https://doi.org/10.1029/2018JB015656

Helmstetter, A., & Shaw, B. E. (2009). Afterslip and aftershocks in the rate-and-state friction law. *Journal of Geophysical Research*, *114*, B01308. https://doi.org/10.1029/2007JB005077

Houston, H. (2015). Low friction and fault weakening revealed by rising sensitivity of tremor to tidal stress. *Nature Geoscience*, *8*(5), 409–415. https://doi.org/10.1038/ngeo2419

Johnson, C. W., Fu, Y., & Bürgmann, R. (2017). Seasonal water storage, stress modulation, and California seismicity. *Science*, *356*(6343), 1161–1164. https://doi.org/10.1126/science.aak9547

Johnson, C. W., Fu, Y., & Bürgmann, R. (2020). Hydrospheric modulation of stress and seismicity on shallow faults in Southern Alaska. *Earth and Planetary Science Letters*, *530*, 115904. https://doi.org/10.1016/j.epsl.2019.115904

Kaneko, Y., & Lapusta, N. (2008). Variability of earthquake nucleation in continuum models of rate-and-state faults and implications for aftershock rates. *Journal of Geophysical Research*, *113*, B12312. https://doi.org/10.1029/2007JB005154

Linker, M. F., & Dieterich, J. H. (1992). Effects of variable normal stress on rock friction: Observations and constitutive equations. *Journal of Geophysical Research*, *97*(B4), 4923–4940. https://doi.org/10.1029/92JB00017

Lognonne, P. (2005). Planetary seismology. *Annual Review of Earth and Planetary Sciences*, *33*(1), 571–604. https://doi.org/10.1146/annurev.earth.33.092203.122604

Lu, Z., Yi, H., & Wen, L. (2018). Loading-induced Earth's stress change over time. *Journal of Geophysical Research: Solid Earth*, *123*, 4285–4306. https://doi.org/10.1029/2017JB015243

Luo, Y., & Liu, Z. (2019). Slow-slip recurrent pattern changes: Perturbation responding and possible scenarios of precursor toward a megathrust earthquake. *Geochemistry, Geophysics, Geosystems*, *20*, 852–871. https://doi.org/10.1029/2018GC008021

Manga, M., Zhai, G., & Wang, C.-Y. (2019). Squeezing marsquakes out of groundwater. *Geophysical Research Letters*, *46*, 6333–6340. https://doi.org/10.1029/2019GL082892

Milbert, D. (2018). Solid. version update used: 2018-Jun-07 https://geodesyworld.github.io/SOFTS/solid.htm

Ross, Z. E., Trugman, D. T., Hauksson, E., & Shearer, P. M. (2019). Searching for hidden earthquakes in Southern California. *Science*, *364*(6442), 767–771. https://doi.org/10.1126/science.aaw6888

Rubin, A. M., & Ampuero, J.-P. (2005). Earthquake nucleation on (aging) rate and state faults. *Journal of Geophysical Research*, *110*, B11312. https://doi.org/10.1029/2005JB003686

Rubinstein, J. L., La Rocca, M., Vidale, J. E., Creager, K. C., & Wech, A. G. (2008). Tidal modulation of nonvolcanic tremor. *Science*, *319*(5860), 186–189. https://doi.org/10.1126/science.1150558

Scholz, C. H., Tan, Y. J., & Albino, F. (2019). The mechanism of tidal triggering of earthquakes at mid-ocean ridges. *Nature communications*, *10*(1), 2526. https://doi.org/10.1038/s41467-019-10605-2

Tanaka, S. (2012). Tidal triggering of earthquakes prior to the 2011 Tohoku-Oki earthquake (*Mw* 9.1). *Geophysical Research Letters*, *39*, L00G26. https://doi.org/10.1029/2012GL051179

Tanaka, S., Ohtake, M., & Sato, H. (2002). Evidence for tidal triggering of earthquakes as revealed from statistical analysis of global data. *Journal of Geophysical Research*, *107*, 2211. https://doi.org/10.1029/2001JB001577

Tanaka, Y., Yabe, S., & Ide, S. (2015). An estimate of tidal and non-tidal modulations of plate subduction speed in the transition zone in the Tokai district. *Earth, Planets and Space*, *67*(1), 1–11. https://doi.org/10.1186/s40623-015-0311-2

Thomas, A. M., Bürgmann, R., Shelly, D. R., Beeler, N. M., & Rudolph, M. L. (2012). Tidal triggering of low frequency earthquakes near Parkfield, California: Implications for fault mechanics within the brittle-ductile transition. *Journal of Geophysical Research*, *117*, B05301. https://doi.org/10.1029/2011JB009036

Thomas, A. M., Nadeau, R. M., & Bürgmann, R. (2009). Tremor-tide correlations and near-lithostatic pore pressure on the deep San Andreas fault. *Nature*, *462*(7276), 1048–1051. https://doi.org/10.1038/nature08654

Tolstoy, M., Vernon, F. L., Orcutt, J. A., & Wyatt, F. K. (2002). Breathing of the seafloor: Tidal correlations of seismicity at Axial volcano. *Geology*, *30*(6), 503–506. https://doi.org/10.1130/0091-7613(2002)030<0503:BOTSTC>2.0.CO;2

Tsuruoka, H., Ohtake, M., & Sato, H. (1995). Statistical test of the tidal triggering of earthquakes: contribution of the ocean tide loading effect. *Geophysical Journal International*, *122*(1), 183–194. https://doi.org/10.1111/j.1365-246X.1995.tb03546.x

Ueda, T., & Kato, A. (2019). Seasonal variations in crustal seismicity in San-in District, Southwest Japan. *Geophysical Research Letters*, *46*, 3172–3179. https://doi.org/10.1029/2018GL081789

Yabe, S., Tanaka, Y., Houston, H., & Ide, S. (2015). Tidal sensitivity of tectonic tremors in Nankai and Cascadia subduction zones. *Journal of Geophysical Research: Solid Earth*, *120*, 7587–7605. https://doi.org/10.1002/2015JB012250